Time series assessment of biocompatibility of decellularized bovine tendon in rat anterior cruciate ligament reconstruction model up to 52 weeks

Masafumi Itoh
Cooperative Major in Advanced Biomedical Sciences, Joint Graduate School of Tokyo Women's Medical University and Waseda University, 2-2 Wakamatsucho, Shinjuku, Tokyo 162-8480, Japan

Hiroki Imasu
Department of Modern Mechanical Engineering, Waseda University, Shinjuku, Tokyo, Japan, 2-2 Wakamatsucho, Shinjuku, Tokyo 162-8480, Japan

Kazuya Takano
Department of Modern Mechanical Engineering, Waseda University, Shinjuku, Tokyo, Japan, 2-2 Wakamatsucho, Shinjuku, Tokyo 162-8480, Japan

Mitsuo Umezu
Department of Modern Mechanical Engineering, Waseda University, Shinjuku, Tokyo, Japan, 2-2 Wakamatsucho, Shinjuku, Tokyo 162-8480, Japan

Ken Okazaki
Department of Orthopedic Surgery, Tokyo Women's Medical University, 8–1, Kawada-Cho, Shinjuku-ku, Tokyo, 162-8666, Japan

Kiyotaka Iwasaki (iwasaki@waseda.jp)
Department of Integrative Bioscience and Biomedical Engineering, Graduate School of Advanced Science and Engineering, Waseda University, Tokyo, Japan

Research Article

Keywords: Decellularization, Xenograft tendon, Anterior cruciate ligament, Biocompatibility

Posted Date: November 3rd, 2021

DOI: https://doi.org/10.21203/rs.3.rs-1030698/v1

Abstract

There is an essential demand for the development of biocompatible graft substitute for knee anterior cruciate ligament reconstruction (ACLR). We aimed to investigate biocompatibility of decellularized bovine-derived tendon using rat knee ACLR model. The Sprague–Dawley rats with 12 weeks old were used. At weeks 1, 2, 4, 8, 16, 26, and 52 (each period, n = 6) after ACLR, rats using decellularized bovine tendon (group D, n = 42) and rats using autologous flexor digitorum longus tendon as a graft (group A, n = 42) were assessed for bone mineral density (BMD) of the peritibial bone tunnel, histology, and immunohistology. BMD increased over time in both groups until week 16 and then maintained without significant group differences. Initially, cellularity in group D was lower than in group A, but by weeks 4–8, both groups were comparable to native anterior cruciate ligament and were maintained until week 52. Initially, group A had more M1 macrophages, which represent inflammation, while group D had more M2 macrophages, which represent tissue regeneration. However, at most periods, the counts of M1 and M2 macrophages were comparable in both groups. This study revealed excellent biocompatibility of the decellularized tendon in the cross-species model.

Introduction

Anterior cruciate ligament (ACL) injury is one of the most common and troublesome injuries of the knee[1]. Due to its poor self-healing ability, the majority of patients who want to return to sports must undergo ACL reconstruction (ACLR) to restore knee stability[2]. In the United States, it has been reported that 200,000 ACL injuries are expected to occur annually, and the direct cost of ACLR was estimated as $3 billion per year[3]. ACLR has used three types of grafts: autograft[4] (using each patient's tissue), allograft[5] (using cadaveric tissue), and artificial synthetic ligament[6]. Autograft is the gold standard graft of ACLR because the clinical outcomes of ACLR using artificial ligament were relatively poor[7] and allograft has its specific problem such as disease transmission[8] and tissue damage by gamma irradiation for sterilization[9]. However, there are still unresolved issues with autograft. To begin with, donor site morbidity, such as anterior knee pain and patella fracture caused by harvesting bone patella tendon-bone graft[10,11], and skin sensory change over the lower leg caused by harvesting medial hamstrings tendon[12]. Second, the graft's volume is insufficient. This issue may arise not only in multiple ligament reconstruction or revision ACLR but also in primary ACLR. ACLR using hamstring grafts < 8 mm in diameter has been reported to have a higher failure rate[13,14]. Furthermore, if the patient is short in stature, the volume of the hamstring may be smaller[15], resulting in a graft < 8 mm in diameter[16]. Third, harvesting autografts from the patient's body would be time-consuming and labor-intensive if done during surgery.

Decellularized tissues from animal sources are attractive because the decellularized tissues have the biological tissue matrix unique to target tissues. The purpose of this study is to investigate the biocompatibility of the decellularized bovine-derived xenograft tendon in a rat ACLR model.

Results

Gross appearance of the femur-graft-tibia complex at each time point

Fig. 1 depicts the gross appearance of the right knee in each time point in representative cases from groups D and A. The decellularized xenograft tissues were retained for 52 weeks in the knee joint.

BMD of peritibial tunnel

Micro-CT images of slices parallel to the tibial tunnel at each time point in each group are shown (Fig. 2-a). There was no significant enlargement of the tibial tunnel in either group over time. In each group, the BMD of the peritibial tunnel increased over time up to week 8 and was plateau after week 16 (Fig. 2-b). There was no significant difference between the groups at each time point. Supplemental videos of the BMD at weeks 4 (Supplementary Video S1) and 52 (Supplementary Video S2) in group D showed that there was no enlargement in tunnel diameter at week 52, and the BMD increased at week 52 than at week 4 at the interface between graft and bone.

Cellularity in the intra-articular graft and intratibial tunnel graft

Fig. 3-a shows the box plots showing the count of cells in the intra-articular graft of group D and group A at each period and group N (native ACL, day 0). At week 1, the cellularity of group D was lower than of group A ($p = 0.01$), and both groups were lower than of group N ($p = 0.007$, $p = 0.01$, respectively). At week 2, there was no longer a significant difference between groups A and D due to increased cellularity in group D. Nonetheless, both groups D and A were lower than group N ($p = 0.007$ and $p = 0.02$, respectively). At week 4, there was no significant difference between groups D and N due to increased cellularity in group D. On the other hand, the cellularity was significantly lower in group A than in group N ($p = 0.007$). At week 8, because the cellularity of both groups A and D increased further, no significant difference was shown between the three groups. After week 16, the cellularity of the three groups became comparable and was maintained thereafter. Fig. 3-b depicts cell infiltration into the intra-articular graft at various time points in representative cases from groups D and A. At week 1, there was a small number of infiltrated cells in group D. At week 2, cell infiltration increased in group D. At week 4, cell infiltration further increased in group D. Cell infiltration increased further in both groups by week 8. Furthermore, cells with oval or rod-shaped nuclei were present in the graft at week 4. Following that, the proportion of cells in the graft with oval or rod-shaped nuclei increased even more, and they were aligned longitudinally in parallel with regularly oriented fibers.

Fig. 3-c shows the box plots showing the count of cells into the intratibial tunnel graft of group D, group A, and group N. At week 1, the count of cells in group D was lower than in group A ($p = 0.04$), and both groups A and D were lower than in group N ($p < 0.0001$, $p < 0.0001$, respectively). At week 2, the cell count of both group D and group A increased, and no significant difference was found between the groups D and A. The number of cells in both groups, however, was significantly lower than in group N ($p = 0.01$, $p = 0.0008$, respectively). After week 4, there was no significant difference between the three groups, and this was maintained until week 52. Fig. 3-d depicts cell infiltration into the intratibial tunnel graft at different time points in representative cases of group D and group A. At week 1, there was a small number of

infiltrated cells in group D. At week 2, cell infiltration increased in both groups. At week 4, cell infiltration further increased in both groups and the cellularity appeared to be comparable. At week 8, cells with oval or rod-shaped nuclei appeared, which were then aligned longitudinally and oriented in parallel with collagen fibers in group D. After week 26, almost all cells were rod-shaped or oval nuclei and aligned longitudinally in parallel with regularly oriented fibers in groups D and A.

Count of M1 and M2 macrophages in decellularized bovine and autologous tendons in the intra-articular and intratibial bone tunnel sites.

The count of M1 macrophages of groups D and A in intra-articular grafts at each time point is shown (Fig. 4-a). The number of M1 macrophages in group D was significantly lower than in group A at week 1 ($p = 0.03$). Week 2 was significantly higher than week 1 for both groups ($p = 0.04$, $p = 0.04$, respectively). Group A tended to be higher than group D, but the difference was not significant ($p = 0.08$). At weeks 4 and 8, no significant difference was present between the groups. At week 16, group D was significantly lower than that group A ($p = 0.002$). At weeks 26 and 52, no significant difference was present between the groups. After the mid-term, a non-significant downward trend in the count of M1 macrophages was observed in both groups.

The count of M1 macrophage in the intratibial tunnel graft of both groups at each time point is shown (Fig. 4-b). At week 1, no significant difference was found between the groups D and A. In comparison to week 1, group A increased numerically but with no statistical significance in week 2, whereas group D showed a significant increase ($p=0.003$). At weeks 2 and 4, there was no significant difference between the groups. Group D was significantly lower than group A at week 8 ($p = 0.046$). After week 16, there was no significant difference between the groups. Group A decreased numerically with no statistical significance at week 52 compared to week 26, while group D decreased with statistical significance ($p = 0.02$).

The count of M2 macrophage of both groups in the intra-articular-graft at each time point is shown (Fig. 4-c). At weeks 1, 2, there was no significant difference between the groups. At week 4, both groups increased significantly compared to week 2 ($p = 0.01$, $p = 0.01$, respectively). Furthermore, group D was significantly higher than group A ($p = 0.002$). After week 8, there was no significant difference between the groups.

At each time point, the count of M2 macrophages of both groups in the intratibial tunnel graft is shown (Fig. 4-d). At week 1, there was no significant difference between the groups. At week 2, both groups increased significantly compared to week 1 ($p = 0.01$, 0.007, respectively), with no significant difference between the groups. At week 8, group D tended to be numerically higher than group A with no statistical significance ($p = 0.08$). After week 8, the count of M2 was maintained and comparable between the groups.

Discussion

The most important finding of this study was that decellularized bovine-derived tendons were repopulated with recipient rat cells and the grafts were retained for 52 weeks, as were autologous grafts in the rat ACLR model.

First, the BMD of the peritibial tunnel in groups D and A was comparable at each time point, increased up to 16 weeks, and then stabilized. One of the causes of early graft failure is the failure of osteointegration into the graft[17]. The success of the healing phase of osteointegration into the graft coincided with an improvement in load-to-failure[18]. Therefore, tendon-bone healing is one of the key points in the success of ACLR[19]. Tendon-bone healing starts with the infiltration of loose, unorganized fibrovascular tissue into the gap between the tendon and bone tunnel, followed by the expression of osteoinductive factors like bone morphogenetic proteins (BMPs)[20,21]. After four weeks, the bone tunnel wall surrounding the tendon graft thickens even more[19,20]. Later, Sharpey-like fibers, considered to be the earliest sign of osteointegration into the tendon[22-24] appear and connect the bone and tendon. It has been reported that allograft tendons may have inferior remodeling in bone tunnels compared to autograft in ACLR in humans[25]. However, our study revealed that the BMD of decellularized bovine tendon xenograft and rat autograft at peritibial tunnels was comparable over time. The decellularized bovine tendon demonstrated autograft-like bone-tendon healing.

The cellularity of the graft of intra-articular and intratibial regions became comparable in both groups after weeks 4, 8 respectively, equivalent to native ACL. It is important to note that the cellularity of group D did not exceed that of group A at weeks 1 and 2. Because if the decellularization was inadequate, there may be many inflammation-derived cells infiltrating in the xenograft in the early stage, and the cellularity of the decellularized xenograft might exceed that of the autologous graft[26-28]. The fact that cellularity in both intra-articular and intratibial tunnel grafts in group A was lower at weeks 1 and 2 than in group N could be attributed to graft necrosis[18,29-32]. Kondo et al.[32] reported that two weeks after ACLR in sheep, the core of an autologous semitendinosus graft was nearly acellular. They concluded that the graft necrosis occurred at week 2, followed by revascularization and cellular infiltration over time, resulting in graft regeneration. The cellularity in group A was lowest at week 1, but it was not acellular. In terms of tissue regeneration, rats are most likely ahead of sheep[33]. As a result, the autologous tendon's cellularity may be lowest before week 1 or between weeks 1 and 2. Furthermore, in the sheep model, the orientation of cells with rod-shaped or oval nuclei began to appear in the grafts at week 12[32], whereas in the current study, the orientation of cells began to appear at week 8. It is also important to note that the cellularity in group D was maintained after reaching the equivalent level to that in group N. If the number of cells in group D increased far exceeding that in group N, the decellularized graft might become cancerous[34-36]. Therefore, the decellularized bovine tendon grafts were considered safely integrated as a new ACL in rats.

M1 macrophages have been reported to be activated by type I cytokines such as interferon-γ (IFN-γ) and tumor necrosis factor-α (TNF-α), and have anti-proliferative, cytotoxic, and pro-inflammatory activities[37-43]. In contrast, M2 macrophages have been reported to suppress the production of pro-inflammatory cytokines and have angiogenic and tissue repair properties[42-45]. During the healing process, these

macrophages can plastically change their polarity in response to local stimuli[42,46,47]. Brown et al.[48] compared four groups of rats that received four types of tissue transplanted into abdominal wall defects: cellular autograft, acellular allograft, cellular xenograft, and acellular xenograft. They observed that the acellular tissue transplant group showed a constructive M2-type remodeling response, while the cellular tissue transplant group showed an M1-dominant strong inflammatory response, resulting in connective tissue deposits and scarring, and indicated that transplantation of tissue containing cellular components, even if they are autologous, causes an M1-type inflammatory response. Previous studies in tendon injuries reported similar results to the current study, with a large increase in the count of M1 macrophages in the first two weeks[49,50], implying that M1 macrophages were involved in acute inflammation[49,51]. Similarly to Brown's study[48], M1 macrophage-dominated inflammation was observed in group A, particularly in the early stages, until the cells in the graft disappeared even if they were autologous cells. Group D had fewer M1 macrophages than group A in early periods. Therefore, group D may have fewer M1 macrophages in intra-articular graft than group A at week 16.

In a rat's Achilles tendon repair model, Sugg et al.[49] reported that the concentration of M2 macrophages became significant at 28 days. Similarly, Kawamura et al.[52] found that M2 macrophages reached maximum accumulation by day 28 in a study of bone to autologous tendons healing using the rat ACLR model. In the current study, the number of M2 macrophages was highest at week 4 in both groups for intra-articular grafts and intratibial tunnel grafts, as previously reported. Several studies have reported that increase of M2 macrophage was associated with promotion of tendon healing[53,54]. Barboni et al.[53] reported that transplantation of human amniotic epithelial cells into injured Achilles tendons of sheep increased the expression of M2-related genes and promoted angiogenesis and extracellular matrix (ECM) remodeling. Gelberman et al. found that flexor tendon repair in dogs with adipose-derived mesenchymal stromal cells (ASCs) and recombinant bone morphogenetic protein-12 resulted in increased levels of M2 macrophages, decreased levels of inflammation, and increased levels of proteins involved in ECM production[54]. In this study, significantly more M2 macrophages appeared in group D in the intra-articular grafts at week 4, and numerically more M2 macrophages appeared in the intratibial tunnel grafts at week 8. Throughout the study, the number of M2 macrophages of group D both in intra-articular and intratibial tunnel grafts was never lower than that of group A. This data indicated that the decellularized tendon might be a better graft than the autologous tendon.

This study has several limitations. First, the biomechanical properties of explanted decellularized tendons and autologous tendons were not tested, because of extensively small size of the rat knee. Indeed, to obtain reliable data in tensile tests, it is necessary to develop chucks for the femur and tibia so that the tissue can be placed horizontally with the tensile direction. We are currently conducting ACLR using a bovine-derived decellularized tendon in sheep. Therefore, biomechanical remodeling properties of the decellularized tendon will be evaluated in the experiments.

Secondly, it is unclear whether the observation period of 52 weeks in rats is sufficient to evaluate thorough in vivo remodeling processes. The remodeling period of the ACLR has been reported to be 12–

24 months in the human autologous hamstring tendon and 6–12 months in the autologous bone-patellar tendon graft[55]. Fifty-two weeks exceeds the remodeling period of the human bone-patellar tendon graft but falls short of the hamstring tendon remodeling period. However, remodeling is much slower in human grafts than in animals[56]. Therefore, 52 weeks in rats is considered sufficient to evaluate in vivo remodeling processes.

This study revealed that bovine tendon-derived decellularized grafts sterilized with ethylene oxide gas after freeze dry had the excellent time series biocompatibility in the rat ACLR model. The BMD of the peritibial tunnel increased over time, equivalent to that of the autologous tendon. Cell infiltration occurred over time, equivalent to that of the autologous tendon. Moreover, the number of M2 macrophages, which are responsible for tissue repair, tended to be higher at 4–8 weeks after ACLR in the decellularized xenograft tendon than in the autologous tendon. These findings encouraged us to further study the potential of the decellularized tendon in a cross-species large-animal model.

Methods

Ethics on Animal Experiments

This study was approved by the Animal Research Ethics Committee of Waseda University (approved number: 2015-A021). All animal experiments complied with the Animal Research: Reporting of *In Vivo* Experiments (ARRIVE) guidelines and were carried out following the National Institutes of Health guide for the care and use of laboratory animals (NIH publications No. 8023, revised 1978).

Preparation of decellularized tendon

Bovine tendons were decellularized using the following procedure[57]. Bovine tendon was incorporated into the pulsatile circulation pf physiological saline solution with 1wt% of sodium deoxycholate (Sigma), under a mean flow and pressure of 5L/min and 80 mmHg, respectively. A microwave was irradiated simultaneously. The temperature of the circulating solution was maintained below 37 degrees Celsius, not to induce thermal denaturation to the tissues. The tissues were then treated with Benzonase^{Ò} nuclease (Merck). The decellularized tissues (Fig. 5-a) were freeze-dried, and then sterilized with ethylene oxide. The tissues were rehydrated with physiological saline solution before use as grafts (Fig. 5-b). The residual amount of DNA in the decellularized tendon were assessed using Quant-iT™ PicoGreen^{Ò} ds-DNA Assay Kit (Invitrogen). The decellularized tissues had a DNA residue of less than 1 ng/mg dry weight, which is significantly less than the value of 50 ng/mg recognized as a safety threshold for decellularized tissue DNA residue[58].

Experimental animal and evaluation period

Male Sprague–Dawley rats (12 weeks old, 350 ± 50 g) were used for ACLR of the right knee. The rats were divided into two groups: group D in which decellularized bovine tendon-derived tissue was used as a graft for ACLR (n = 42), and group A in which the autologous flexor digitorum longus tendon of the right

hind limb was used as a graft for ACLR (n = 42). Each group was evaluated at weeks 1, 2, 4, 8, 16, 26, and 52 after ACLR with six animals in each period. The bone mineral density (BMD) of the right per-tibial tunnel and the cellularity of the native ACL of the left knee were assessed in six animals with a 0-day implantation period (group N), for a total of 90 rats.

ACLR in rat

ACLR in rats was performed based on the methods of previous studies[52,59]. General anesthesia was induced by intraperitoneal injection of 60 mg/kg of sodium pentobarbital (Kyoritsu Seiyaku, Tokyo, Japan). If insufficient, additional doses of 6.5 mg each were administered, not to overdose. As a preventative measure, 4 mg/kg of cefazolin sodium (LTL pharma, Tokyo, Japan) was injected intraperitoneally. In group D, decellularized bovine tendon were trimmed in a diameter of 1.5 mm and a length of 15 mm, with the longitudinal diameter parallel to the fiber direction. In group A, a longitudinal incision was made on the medial side of the ipsilateral lower leg, from which the flexor digitorum longus tendon was harvested at a size of approximately 1.5 mm in diameter and 15 mm in length. In each group, a 3-0 silk thread (Akiyama medical, Tokyo, Japan) was sutured at both ends of the graft. Following that, the procedure was the same in both groups. The ACL was resected in its natural state. A 1.8-mm diameter Kirschner-wire was used to create the femoral tunnel from the footprint of the native ACL to the lateral femoral epicondyle. The tibial tunnel was created in the same way. The graft was inserted into the tunnels, and silk thread was secured to the periosteum around each tunnel aperture, being careful not to loosen the graft (Fig. 5-c,d). The joint capsule and skin were sutured using 5-0 nylon thread (Alfresa Pharma Corporation, Osaka, Japan). Immediately after surgery, the rats were transferred to a warm cage and allowed to move freely upon awakening from anesthesia. All rats did not develop any complications during the observation period.

Sample harvest

Six rats were euthanized with an overdose of sodium pentobarbital via intraperitoneal injection at the time specified above. The meniscus and other ligaments were carefully removed from the femur-graft-tibia complex. The samples were fixed in 10% formalin solution at 4°C after rinsing the blood thoroughly with saline.

Measurement of BMD of the peritibial tunnel using micro-CT

CT images of the femur-graft-tibia complex were taken using a 3-D measuring X-ray CT scanner (TDM 1300-IS, Yamato Scientific Co., Ltd, Tokyo, Japan) (set voltage: 45 kV, set current: 236,0 μA, filter: 0.1 mm brass plate, acquisition time: 10 min) to evaluate the overtime peritunnel bone reconstruction at the interface between the graft and the tibial tunnel. Under the same conditions, phantoms of known density were imaged, and calibration curves were obtained. Based on the calibration curve, 3D BON (RATOC system engineering Co., Ltd, Tokyo, Japan) was used to analyze the BMD. In a slice along the long axis of the tibial tunnel, the BMD was measured at the top, middle, and bottom of a region 2 mm distal to the tibial epiphyseal plate (Fig. 6).

Histology

After micro-CT imaging, samples were decalcified with 9% formic acid for 4–6 weeks and then embedded in paraffin. 5-μm-thick longitudinal paraffin sections parallel to the direction of the tibial tunnel and intra-articular graft, and which parallel to the femoral tunnel were prepared[59] and stained with hematoxylin-eosin (HE). Fluorescence microscopy (BZ-8100, KEYENCE, Osaka, Japan) was used to observe the whole image (magnification ×2) and local view (magnification ×200). The graft between the apertures of the femoral and tibial tunnels was defined as the “intra-articular graft.” The term “intratibial tunnel graft” refers to a graft that enters the tibial tunnel deeper than the tibial tunnel aperture. To assess the cellularity of the graft, the cells inside the intratibial tunnel graft and the intra-articular graft were counted.

Immunohistochemical study for macrophage infiltration into the graft

Immunohistochemical staining was performed to investigate the phenotype[48] of macrophages (M1, M2) that accumulate in the grafts. Rabbit anti-CCR7 (Cell Applications, San Diego, CA) was used for M1 macrophage staining, and mouse anti-rat CD163 (Serotec) was used for M2 macrophage staining. The staining was done with reference to the previous study[48]. The macrophages of each phenotype infiltrating the intratibial tunnel graft and in the intra-articular graft were counted.

Cell count

The entire tissue was observed on a slide using a fluorescence microscope (Fig. 7-a). Both in the core of the intra-articular graft approximately equidistant from the tibial and femoral tunnel apertures (Fig. 7-b) and in the core of the intratibial tunnel graft from the tibial tunnel aperture distally (Fig. 7-c), cells in the grafts were counted. The number of cells were counted using Image-J software[60] in six 200-μm^2 square regions, respectively. Then, the average number in the six squares was used. The number of cells in the native ACL of the left knee was counted (n = 6) using the same protocol. In immunohistochemical staining, the number of M1 and M2 macrophages were counted using the same protocol (Fig. 7-d,e,f).

Statistical Analysis

Box-and-whisker plots were used to display the distribution of each data. The Shapiro–Wilk W test was used to test the normality of continuous variables. Depending on whether the distribution is normal or not, the student t-test or Mann–Whitney U test was used to compare the mean differences between the two groups. Depending on whether the distribution is normal or not, the Kruskal–Wallis test or one-way analysis of variance was used to compare the means of the three groups. When there was a significant difference in the three groups, the student t-test or the Mann–Whitney U test was used to evaluate the difference in the means of each group as a post hoc analysis. Holm’s multiple comparison method was used for the p-value correction. $P < 0.05$ was considered statistically significant. JMP Pro version 13.2.1 (SAS, Cary, NC, USA) was used for statistical analyses.

Declarations

Data availability

All data generated or analyzed during this study are included in this published article.

Acknowledgments

The authors would like to thank Takuto Yoshinaga and Toshiaki Yamano for their assistance with the animal experiment and thank Enago (www.enago.jp) for the English language review.

Author contributions

M.I. designed the study, performed experiments, analyzed, interpreted, and wrote the original draft. H.I. and K.T. performed experiments and analyzed. M. U. and K.O. supervised. K.I. conceptualized, designed study, performed experiments, interpreted, critically revised the original draft, and supervised.

Funding

This study was supported by A-STEP (Adaptable and seamless technology transfer program through target-driven R&D) Feasibility Stage (No. AS231Z04918F), Japan Science and Technology Agency.

Competing interests

The authors declare no competing interests.

Additional information

Correspondence and requests for materials should be addressed to K.I.

References

1. Parkkari, J., Pasanen, K., Mattila, V. M., Kannus, P. & Rimpelä, A. The risk for a cruciate ligament injury of the knee in adolescents and young adults: a population-based cohort study of 46500 people with a 9 year follow-up. *Br. J. Sports Med.* **42**, 422–426 (2008).10.1136/bjsm.2008.046185, Pubmed:18390920

2. Moksnes, H., Engebretsen, L. & Risberg, M. A. Performance-based functional outcome for children 12 years or younger following anterior cruciate ligament injury: a two to nine-year follow-up study. *Knee Surg. Sports Traumatol. Arthrosc.* **16**, 214–223 (2008).10.1007/s00167-007-0469-7, Pubmed:18157486

3. Brophy, R. H., Wright, R. W. & Matava, M. J. Cost analysis of converting from single-bundle to double-bundle anterior cruciate ligament reconstruction. *Am. J. Sports Med.* **37**, 683–687 (2009).10.1177/0363546508328121, Pubmed:19204364

4. Mohtadi, N. G. H., Chan, D. S., Dainty, K. N. & Whelan, D. B. Patellar tendon versus hamstring tendon autograft for anterior cruciate ligament rupture in adults. *Cochrane DatabaseSyst. Rev.* (9), CD005960 (2011).10.1002/14651858.CD005960.pub2, Pubmed:21901700

5. Shino, K., Oakes, B. W., Horibe, S., Nakata, K. & Nakamura, N. Collagen fibril populations in human anterior cruciate ligament allografts. Electron microscopic analysis. *Am. J. Sports Med.* **23**, 203–208; discussion 209 (1995).10.1177/036354659502300213, Pubmed:7778706

6. Hamido, F. *et al*. The use of the LARS artificial ligament to augment a short or undersized ACL hamstrings tendon graft. *Knee* **18**, 373–378 (2011).10.1016/j.knee.2010.09.003, Pubmed:21062673

7. Schroven, I. T., Geens, S., Beckers, L., Lagrange, W. & Fabry, G. Experience with the Leeds-Keio artificial ligament for anterior cruciate ligament reconstruction. *Knee Surg. Sports Traumatol. Arthrosc.* **2**, 214–218 (1994).10.1007/BF01845590, Pubmed:8536043

8. Patel, R. & Trampuz, A. Infections transmitted through musculoskeletal-tissue allografts. *N.Engl.J.Med.* **350**, 2544–2546 (2004).10.1056/NEJMp048090, Pubmed:15201409

9. Hulet, C. *et al*. The use of allograft tendons in primary ACL reconstruction. *Knee Surg. Sports Traumatol. Arthrosc.* **27**, 1754–1770 (2019).10.1007/s00167-019-05440-3, Pubmed:30830297

10. Christen, B. & Jakob, R. P. Fractures associated with patellar ligament grafts in cruciate ligament surgery. *J.Bone Joint Surg.Br.* **74**, 617–619 (1992).10.1302/0301-620X.74B4.1624526, Pubmed:1624526

11. Breitfuss, H., Fröhlich, R., Povacz, P., Resch, H. & Wicker, A. The tendon defect after anterior cruciate ligament reconstruction using the midthird patellar tendon-a problem for the patellofemoral joint? *KneeSurg. Sports Traumatol. Arthrosc.* **3**, 194–198 (1996).10.1007/BF01466615, Pubmed:8739711

12. Mochizuki, T., Muneta, T., Yagishita, K., Shinomiya, K. & Sekiya, I. Skin sensory change after arthroscopically-assisted anterior cruciate ligament reconstruction using medial hamstring tendons with a vertical incision. *Knee Surg. Sports Traumatol. Arthrosc.* **12**, 198–202 (2004).10.1007/s00167-003-0451-y, Pubmed:14625669

13. Conte, E. J., Hyatt, A. E., Gatt, C. J., Jr & Dhawan, A. Hamstring autograft size can be predicted and is a potential risk factor for anterior cruciate ligament reconstruction failure. *Arthroscopy* **30**, 882–890 (2014).10.1016/j.arthro.2014.03.028, Pubmed:24951356

14. Park, S. Y. *et al*. Factors predicting hamstring tendon autograft diameters and resulting failure rates after anterior cruciate ligament reconstruction. *Knee Surg. Sports Traumatol. Arthrosc.* **21**, 1111–1118 (2013).10.1007/s00167-012-2085-4, Pubmed:22688502

15. Tuman, J. M. *et al*. Predictors for hamstring graft diameter in anterior cruciate ligament reconstruction. *Am. J. Sports Med.* **35**, 1945–1949 (2007).10.1177/0363546507304667, Pubmed:17644660

16. Brown, C. H., Jr. Editorial commentary: how to increase hamstring tendon graft size for anterior cruciate ligament reconstruction. *Arthroscopy* **34**, 2641–2646 (2018).10.1016/j.arthro.2018.06.014, Pubmed:30173804

17. George, M. S., Dunn, W. R. & Spindler, K. P. Current concepts review: revision anterior cruciate ligament reconstruction. *Am. J. Sports Med.* **34**, 2026–2037 (2006).10.1177/0363546506295026, Pubmed:17092921

18. Yao, S., Fu, B. S. & Yung, P. S. Graft healing after anterior cruciate ligament reconstruction (ACLR). *Asia Pac.J.Sports Med.Arthrosc.Rehabil.Technol.* **25**, 8–15 (2021).10.1016/j.asmart.2021.03.003, Pubmed:34094881

19. Ekdahl, M., Wang, J. H., Ronga, M. & Fu, F. H. Graft healing in anterior cruciate ligament reconstruction. *Knee Surg. Sports Traumatol. Arthrosc.* **16**, 935–947 (2008).10.1007/s00167-008-0584-0, Pubmed:18633596

20. Hays, P. L. *et al*. The role of macrophages in early healing of a tendon graft in a bone tunnel. *J. Bone Joint Surg. Am.* **90**, 565–579 (2008).10.2106/JBJS.F.00531, Pubmed:18310707

21. Kobayashi, M. *et al*. The fate of host and graft cells in early healing of bone tunnel after tendon graft. *Am. J. Sports Med.* **33**, 1892–1897 (2005).10.1177/0363546505277140, Pubmed:16157856

22. Liu, S. H. *et al*. Morphology and matrix composition during early tendon to bone healing. *Clin.Orthop.Relat.Res.* (339), 253–260 (1997).10.1097/00003086-199706000-00034, Pubmed:9186227

23. Rodeo, S. A., Arnoczky, S. P., Torzilli, P. A., Hidaka, C. & Warren, R. F. Tendon-healing in a bone tunnel. A biomechanical and histological study in the dog. *J. Bone Joint Surg. Am.* **75**, 1795–1803 (1993).10.2106/00004623-199312000-00009, Pubmed:8258550

24. Rodeo, S. A., Suzuki, K., Deng, X. H., Wozney, J. & Warren, R. F. Use of recombinant human bone morphogenetic protein-2 to enhance tendon healing in a bone tunnel. *Am. J. Sports Med.* **27**, 476–488 (1999).10.1177/03635465990270041201, Pubmed:10424218

25. Ge, Y. *et al*. Comparison of tendon-bone healing between autografts and allografts after anterior cruciate ligament reconstruction using magnetic resonance imaging. *Knee Surg. Sports Traumatol. Arthrosc.* **23**, 954–960 (2015).10.1007/s00167-013-2755-x, Pubmed:24196576

26. Farnebo, S. *et al*. Decellularized tendon-bone composite grafts for extremity reconstruction: an experimental study. *Plast. Reconstr. Surg.* **133**, 79–89 (2014).10.1097/01.prs.0000436823.64827.a0, Pubmed:24374670

27. Gilbert, T. W., Sellaro, T. L. & Badylak, S. F. Decellularization of tissues and organs. *Biomaterials* **27**, 3675–3683 (2006).10.1016/j.biomaterials.2006.02.014, Pubmed:16519932

28. Badylak, S. F. Xenogeneic extracellular matrix as a scaffold for tissue reconstruction. *Transpl.Immunol.* **12**, 367–377 (2004).10.1016/j.trim.2003.12.016, Pubmed:15157928

29. Amiel, D., Kleiner, J. B. & Akeson, W. H. The natural history of the anterior cruciate ligament autograft of patellar tendon origin. *Am. J. Sports Med.* **14**, 449–462 (1986).10.1177/036354658601400603, Pubmed:3799871

30. Arnoczky, S. P., Tarvin, G. B. & Marshall, J. L. Anterior cruciate ligament replacement using patellar tendon. An evaluation of graft revascularization in the dog. *J. Bone Joint Surg. Am.* **64**, 217–224 (1982).10.2106/00004623-198264020-00011, Pubmed:7056776

31. Clancy, W. G. J. *et al*. Anterior and posterior cruciate ligament reconstruction in rhesus monkeys. *J. Bone Joint Surg. Am.* **63**, 1270–1284 (1981).10.2106/00004623-198163080-00008, Pubmed:7287797

32. Kondo, E. *et al*. Biomechanical and histological evaluations of the doubled semitendinosus tendon autograft after anterior cruciate ligament reconstruction in sheep. *Am. J. Sports Med.* **40**, 315–324 (2012).10.1177/0363546511426417, Pubmed:22088579

33. Iismaa, S. E. *et al*. Comparative regenerative mechanisms across different mammalian tissues. *npjRegen.Med.* **3**, 6 (2018).10.1038/s41536-018-0044-5, Pubmed:29507774

34. Donnenberg, V. S., Zimmerlin, L., Rubin, J. P. & Donnenberg, A. D. Regenerative therapy after cancer: what are the risks? *Tissue Eng.Part B Rev.* **16**, 567–575 (2010).10.1089/ten.TEB.2010.0352, Pubmed:20726819

35. Wong, G. S. & Rustgi, A. K. Matricellular proteins: priming the tumour microenvironment for cancer development and metastasis. *Br.J.Cancer* **108**, 755–761 (2013).10.1038/bjc.2012.592, Pubmed:23322204

36. Werb, Z. & Lu, P. The role of stroma in tumor development. *CancerJ.* **21**, 250–253 (2015).10.1097/PPO.0000000000000127, Pubmed:26222075

37. Edwards, J. P., Zhang, X., Frauwirth, K. A. & Mosser, D. M. Biochemical and functional characterization of three activated macrophage populations. *J.Leukoc.Biol.* **80**, 1298–1307 (2006).10.1189/jlb.0406249, Pubmed:16905575

38. Benoit, M., Desnues, B. & Mege, J. L. Macrophage polarization in bacterial infections. *J.Immunol.* **181**, 3733–3739 (2008).10.4049/jimmunol.181.6.3733, Pubmed:18768823

39. Van Ginderachter, J. A. *et al*. Classical and alternative activation of mononuclear phagocytes: picking the best of both worlds for tumor promotion. *Immunobiology* **211**, 487–501 (2006).10.1016/j.imbio.2006.06.002, Pubmed:16920488

40. Laskin, D. L. Macrophages and inflammatory mediators in chemical toxicity: a battle of forces. *Chem.Res.Toxicol.* **22**, 1376–1385 (2009).10.1021/tx900086v, Pubmed:19645497

41. Mantovani, A., Sica, A. & Locati, M. Macrophage polarization comes of age. *Immunity* **23**, 344–346 (2005).10.1016/j.immuni.2005.10.001, Pubmed:16226499

42. Sica, A. & Mantovani, A. Macrophage plasticity and polarization: in vivo veritas. *J.Clin.Invest.* **122**, 787–795 (2012).10.1172/JCI59643, Pubmed:22378047

43. Verreck, F. A., de Boer, T., Langenberg, D. M., van der Zanden, L. & Ottenhoff, T. H. Phenotypic and functional profiling of human proinflammatory type-1 and anti-inflammatory type-2 macrophages in response to microbial antigens and IFN-gamma- and CD40L-mediated costimulation. *J.Leukoc.Biol.* **79**, 285–293 (2006).10.1189/jlb.0105015, Pubmed:16330536

44. Mosser, D. M. The many faces of macrophage activation. *J.Leukoc.Biol.* **73**, 209–212 (2003).10.1189/jlb.0602325, Pubmed:12554797

45. Badylak, S. F., Valentin, J. E., Ravindra, A. K., McCabe, G. P. & Stewart-Akers, A. M. Macrophage phenotype as a determinant of biologic scaffold remodeling. *TissueEng. Part A* **14**, 1835–1842 (2008).10.1089/ten.tea.2007.0264, Pubmed:18950271

46. Porcheray, F. *et al*. Macrophage activation switching: an asset for the resolution of inflammation. *Clin.Exp.Immunol.* **142**, 481–489 (2005).10.1111/j.1365-2249.2005.02934.x, Pubmed:16297160

47. Stout, R. D. *et al*. Macrophages sequentially change their functional phenotype in response to changes in microenvironmental influences. *J. Immunol.* **175**, 342–349 (2005).10.4049/jimmunol.175.1.342, Pubmed:15972667

48. Brown, B. N., Valentin, J. E., Stewart-Akers, A. M., McCabe, G. P. & Badylak, S. F. Macrophage phenotype and remodeling outcomes in response to biologic scaffolds with and without a cellular component. *Biomaterials* **30**, 1482–1491 (2009).10.1016/j.biomaterials.2008.11.040, Pubmed:19121538

49. Sugg, K. B., Lubardic, J., Gumucio, J. P. & Mendias, C. L. Changes in macrophage phenotype and induction of epithelial-to-mesenchymal transition genes following acute Achilles tenotomy and repair. *J. Orthop. Res.* **32**, 944–951 (2014).10.1002/jor.22624, Pubmed:24700411

50. Marsolais, D., Côté, C. H. & Frenette, J. Neutrophils and macrophages accumulate sequentially following Achilles tendon injury. *J. Orthop. Res.* **19**, 1203–1209 (2001).10.1016/S0736-0266(01)00031-6, Pubmed:11781025

51. Matthews, T. J., Hand, G. C., Rees, J. L., Athanasou, N. A. & Carr, A. J. Pathology of the torn rotator cuff tendon. Reduction in potential for repair as tear size increases. *J.Bone Joint Surg.Br.* **88**, 489–495 (2006).10.1302/0301-620X.88B4.16845, Pubmed:16567784

52. Kawamura, S., Ying, L., Kim, H. J., Dynybil, C. & Rodeo, S. A. Macrophages accumulate in the early phase of tendon-bone healing. *J. Orthop. Res.* **23**, 1425–1432 (2005).10.1016/j.orthres.2005.01.014.1100230627, Pubmed:16111854

53. Barboni, B. *et al*. Therapeutic potential of hAECs for early Achilles tendon defect repair through regeneration. *J. Tissue Eng. Regen. Med.* **12**, e1594–e1608 (2018).10.1002/term.2584, Pubmed:29024514

54. Gelberman, R. H. *et al*. Combined administration of ASCs and BMP-12 promotes an M2 macrophage phenotype and enhances tendon healing. *Clin.Orthop.Relat.Res.* **475**, 2318–2331 (2017).10.1007/s11999-017-5369-7, Pubmed:28462460

55. Pauzenberger, L., Syré, S. & Schurz, M.. "Ligamentization" in hamstring tendon grafts after anterior cruciate ligament reconstruction: a systematic review of the literature and a glimpse into the future. *Arthroscopy* **29**, 1712–1721 (2013).10.1016/j.arthro.2013.05.009, Pubmed:23859954

56. Claes, S., Verdonk, P., Forsyth, R. & Bellemans, J. The "ligamentization" process in anterior cruciate ligament reconstruction: what happens to the human graft? A systematic review of the literature. *Am. J. Sports Med.* **39**, 2476–2483 (2011).10.1177/0363546511402662, Pubmed:21515806

57. Iwasaki, K. *et al*. Innovative bioreactor technologies produced a completely decellularized and pre-endothelialized functional aortic valve. *IFMBEProc.* **12** (2005)

58. Crapo, P. M., Gilbert, T. W. & Badylak, S. F. An overview of tissue and whole organ decellularization processes. *Biomaterials* **32**, 3233–3243 (2011).10.1016/j.biomaterials.2011.01.057, Pubmed:21296410

59. Lui, P. P., Lee, Y. W., Mok, T. Y., Cheuk, Y. C. & Chan, K. M. Alendronate reduced peri-tunnel bone loss and enhanced tendon graft to bone tunnel healing in anterior cruciate ligament reconstruction. *Eur. Cell. Mater.* **25**, 78–96 (2013).10.22203/ecm.v025a06, Pubmed:23325540

60. Schneider, C. A., Rasband, W. S. & Eliceiri, K. W. NIH Image to ImageJ: 25 years ofimage analysis. *Nat.Methods* **9**, 671–675 (2012).10.1038/nmeth.2089, Pubmed:22930834

Figures

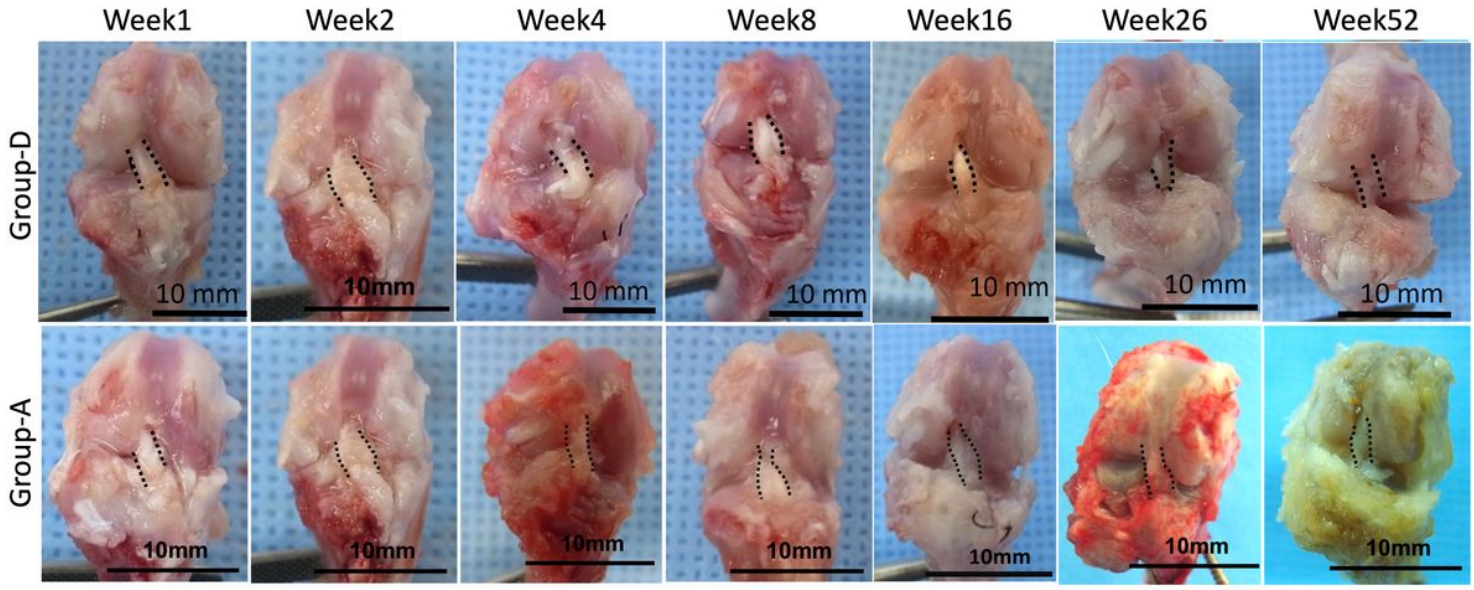

Figure 1

The gross appearance of right knee in representative cases in each time point of group D and group A. The black dashed line shows the outline of the graft. Group D, decellularized bovine tendon graft; group A, autologous tendon graft

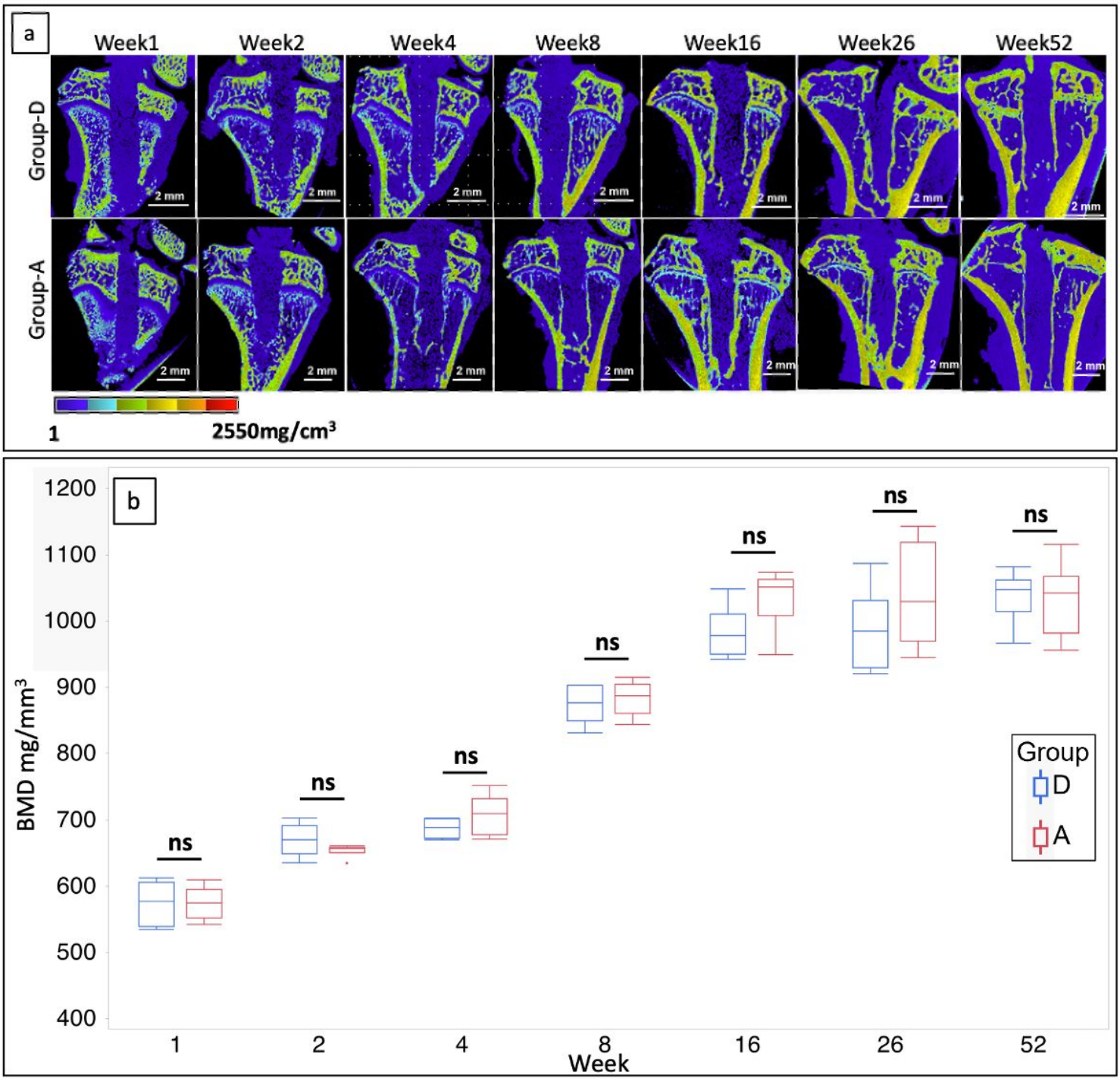

Figure 2

Time series bone mineral density formed at the interface between graft and bone of peritibial tunnel a: The micro-CT images of slices parallel to the tibial tunnel at each time point in each group. b: Box plots showing the BMD of the peritibial tunnel for each group at each time point. BMD, bone mineral density; CT, computed tomography; group D, decellularized bovine tendon graft; group A, autologous tendon graft; ns, not statistically significant

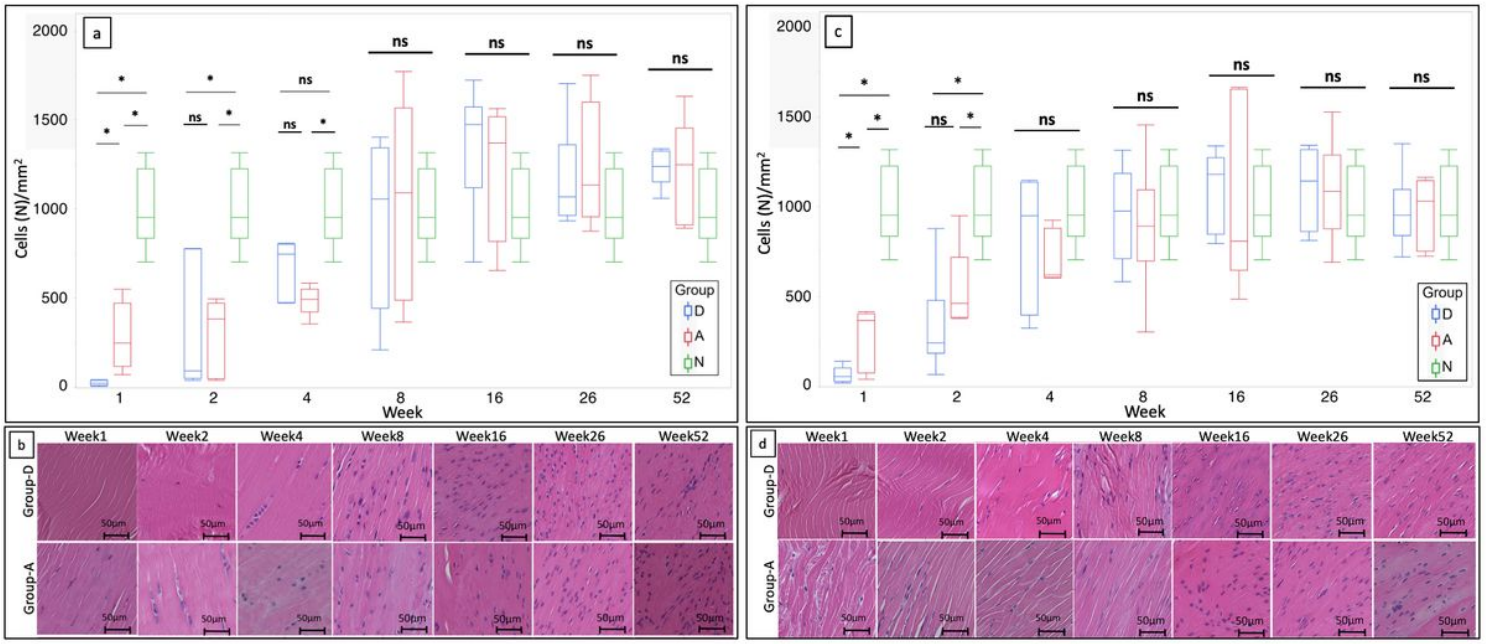

Figure 3

Comparison of cellularity of decellularized bovine tendon and autologous tendon in rat anterior cruciate ligament reconstruction up to 52 weeks of implantation. a: Box plots depicting the count of cells in intra-articular grafts of groups D and A at each time point. The number of cells in native ACL are shown as group N. b: Representative hematoxylin-eosin staining showing cell infiltration in the intra-articular graft at various time points in group D and group A. c: Box plots showing the count of cells in the intratibial tunnel grafts of groups D and A at each period. The number of cells in native ACL are shown as group N. d: Representative hematoxylin-eosin staining showing cell infiltration in the intratibial tunnel graft at various time points in group D and group A. ACL, anterior cruciate ligament; group D, decellularized bovine tendon graft; group A, autologous tendon graft; group N, native ACL; *, statistically significant ($p < 0.05$); ns, not statistically significant

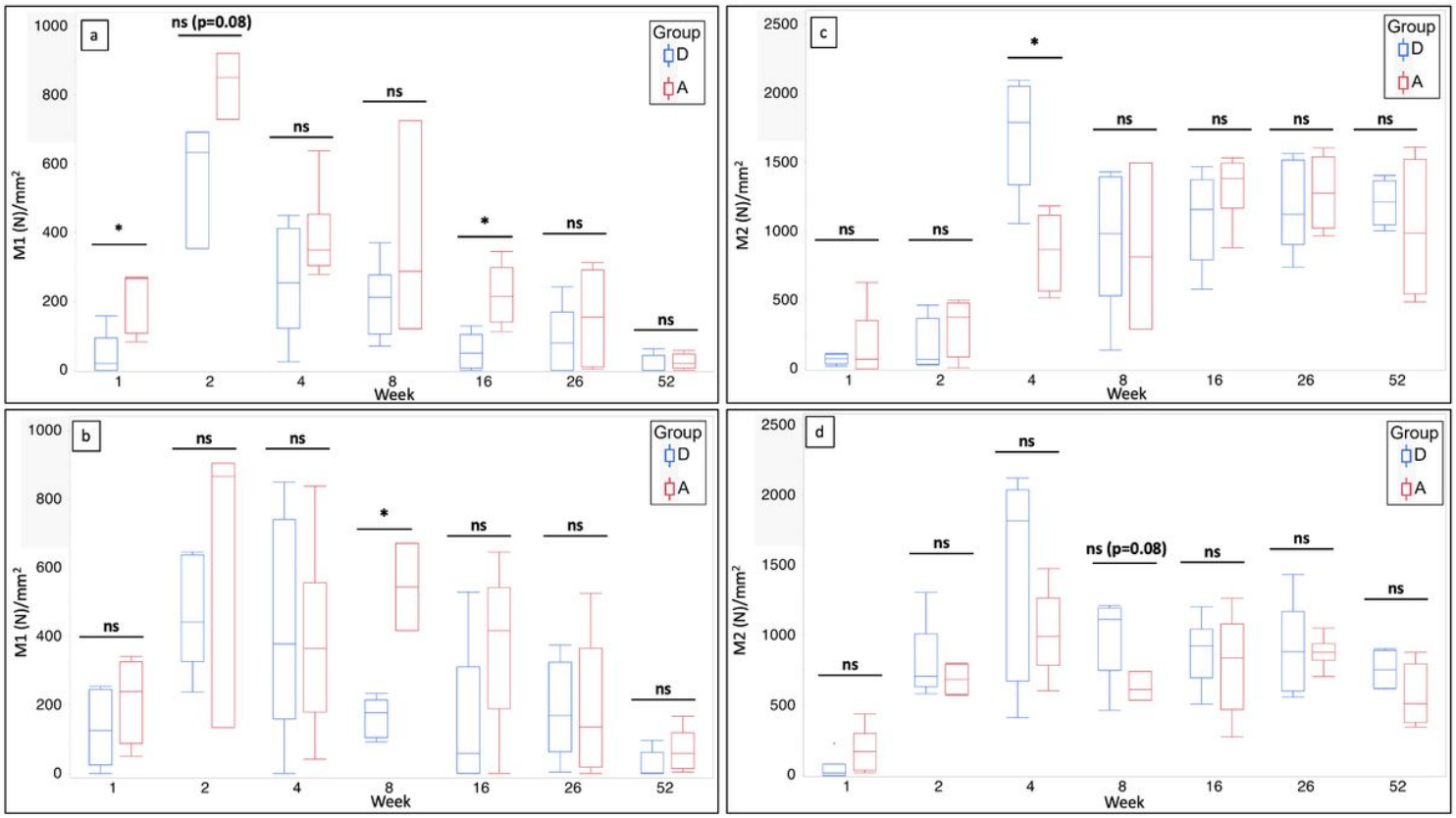

Figure 4

Comparison of time series changes in the count of M1 and M2 macrophages appeared in the decellularized and autologous tendons in rat anterior cruciate ligament reconstruction in the intra-articular graft and intratibial bone tunnel graft a: The box plots showing the count of M1 macrophage of groups D and A in the intra-articular grafts at each time point. b: The box plots showing the count of M1 macrophages of groups D and A in intratibial tunnel grafts at each time point. c: The box plots showing the count of M2 macrophages of groups D and A in the intra-articular grafts at each time point. d: The box plots showing the count of M2 macrophages of groups D and A in intratibial tunnel grafts at each time point. Group D, decellularized bovine tendon graft, group A, autologous tendon graft; group N, native anterior cruciate ligament; *, statistically significant ($p < 0.05$); ns, not statistically significant

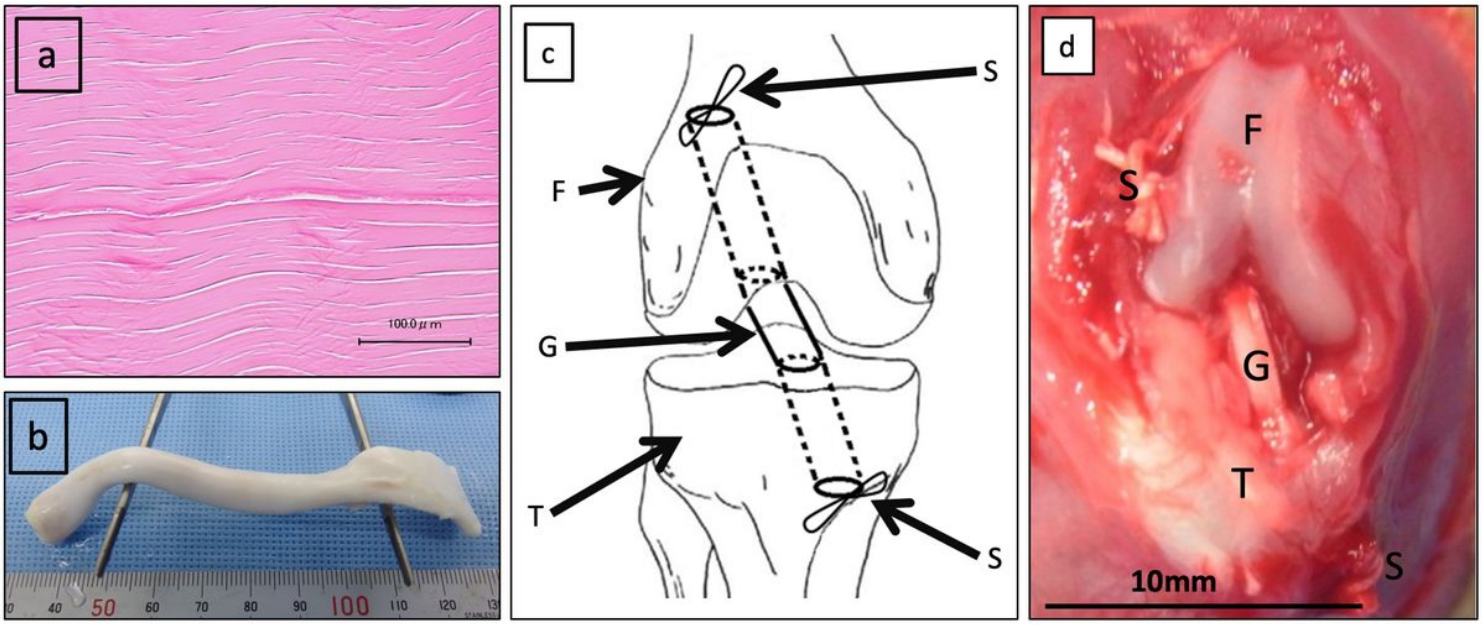

Figure 5

Anterior cruciate ligament reconstruction in rats using the decellularized bovine tendon and autologous tendon grafts. a: Hematoxylin-eosin staining of the decellularized bovine tendon. No cell components can be seen and the extracellular matrix and fiber arrangement are preserved. b: The gross appearance of the decellularized bovine tendon after rehydration with physiological saline solution. c: Schematic diagram of the completion of anterior cruciate ligament reconstruction in a rat. d: Gross appearance of anterior cruciate ligament reconstruction in right knee of the rat at completion. F, femur; T, tibia; G, graft; S, 3-0 silk thread

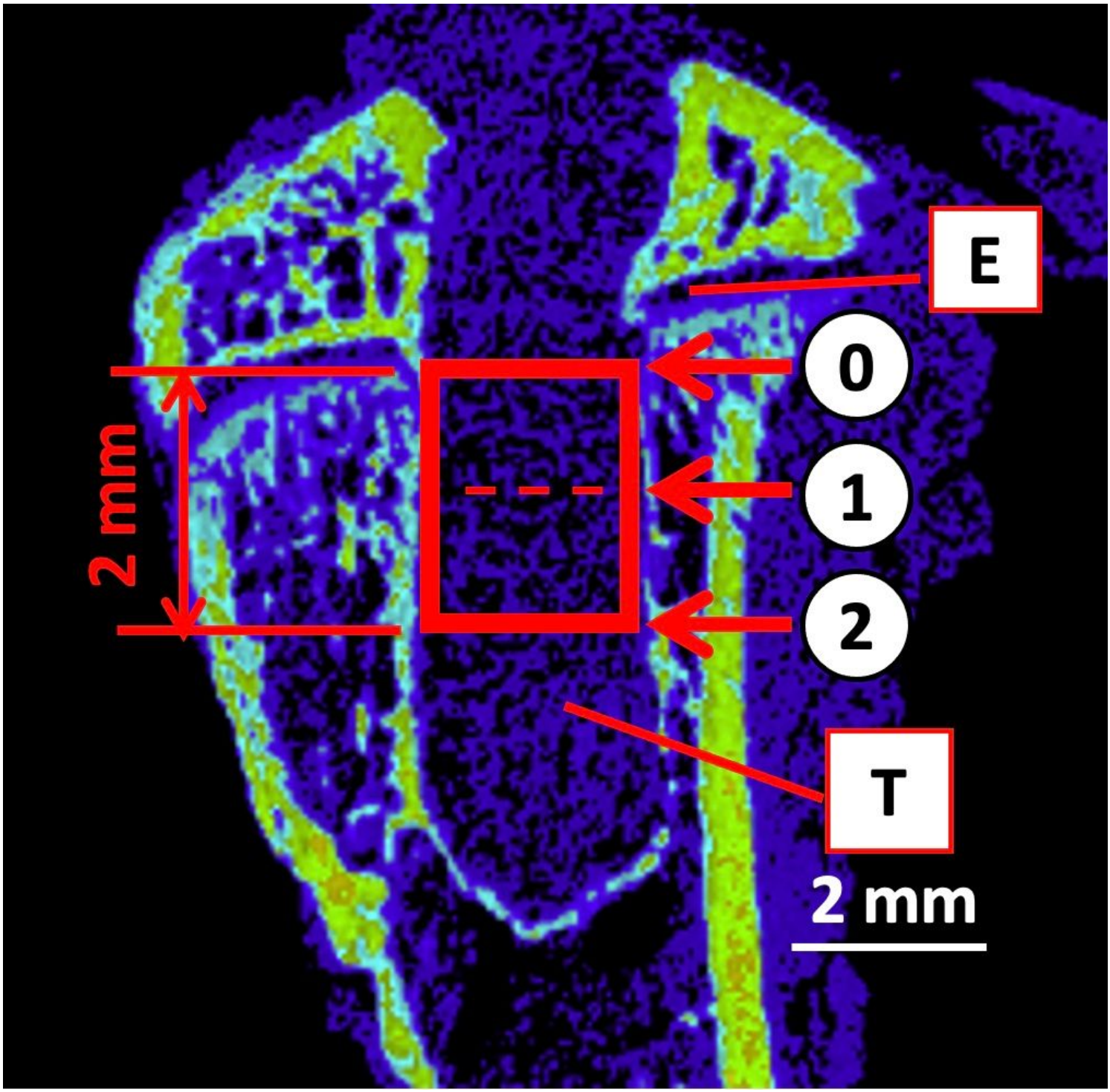

Figure 6

Measurement of bone mineral density at the interface between the graft and tibial tunnel. The definition of the measurement area of bone mineral density. The CT image shows slices along the long axis of the tibial tunnel. The BMD was measured at the top, middle, and bottom of a region 2 mm distal to the tibial epiphyseal plate. The major and minor tunnel diameters were measured at three cross-sections, namely, upper (0), middle (1), and lower (2) ends of the region 2 mm distal to the growth cartilage (red square) in the femur-graft-tibia complex. The data of day 0 after anterior cruciate ligament reconstruction were used

to determine the baseline for the diameter of the hole drilled. CT, computed tomography; E, epiphysis; T, tunnel

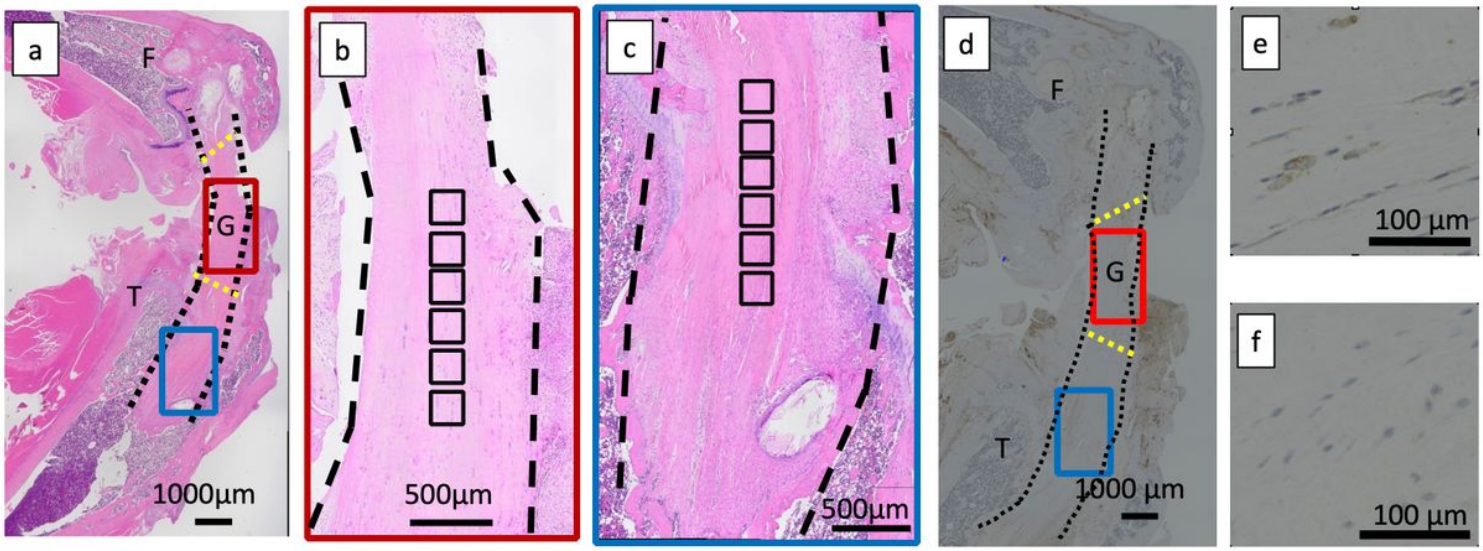

Figure 7

Hematoxylin-eosin staining and immunobiological staining of M1 and M2 macrophages of femur-graft-tibia complex for quantitative evaluation of cells infiltrated into the decellularized and autologous grafts a: Overall view of the femur-graft-tibia complex stained in hematoxylin-eosin. b: Magnified view of the intra-articular graft, magnifying the red rectangle in Fig. 3-a. c: Magnified view of the graft in the tibial tunnel, magnifying the blue rectangle in Fig. 3-a. d: Overall view of immunohistochemical staining of M1 and M2 macrophages in the femur-graft-tibia complex. M1 and M2 macrophages in the intra-articular graft (in the red rectangle) and in the intratibial tunnel graft (in the blue rectangle) are counted by the same method as the Hematoxylin-eosin staining. e: M1 macrophages f: M2 macrophages The black dashed line shows the surface of the graft. The aperture of the bone tunnel into the joint is indicated by the yellow dashed line. One black square in 3-b and 3-c has a surface area of 200 µm2. F, femur; G, graft; T, tibia.

Supplementary Files

This is a list of supplementary files associated with this preprint. Click to download.

- SupplementaryVideoS1.mov
- SupplementaryVideoS2.mov